Materials Today Bio 26 (2024) 101094

Contents lists available at ScienceDirect

Materials Today Bio

journal homepage: www.journals.elsevier.com/materials-today-bio

Neuroprotective effects of anti-TRAIL-ICG nanoagent and its multimodal imaging evaluation in cerebral ischemia-reperfusion injury

Qiong Yang [a,1], Wenxuan Ye [b,1], Doudou Luo [b,1], Jiwei Xing [a], Qingqing Xiao [c], Huiling Wu [a], Youliang Yao [a], Guangxing Wang [a], Luyao Yang [a], Dongbei Guo [a], Kun Wang [d], Yaqin He [e], Xiaofeng Ye [e], Jinde Zhang [f], Zhaokui Jin [g], Zhongxiong Fan [h,**], Xiaofei Wen [a,***], Jingsong Mao [a,c,****], Xiaoyuan Chen [i], Qingliang Zhao [a,*]

[a] *State Key Laboratory of Vaccines for Infectious Diseases, Xiang An Biomedicine Laboratory, Center for Molecular Imaging and Translational Medicine, Department of Vascular & Tumor Interventional Radiology, The First Affiliated Hospital of Xiamen University, School of Medicine, School of Public Health, Xiamen University, Xiamen, 361102, China*

[b] *The First Affiliated Hospital of Xiamen University, School of Medicine, Xiamen University, Xiamen, 361102, China*

[c] *Department of Vascular Intervention, Guilin Medical College Affiliated Hospital, Guilin Medical College, Guilin, 541000, China*

[d] *Key Laboratory of Optoelectronic Science and Technology for Medicine of Ministry of Education, Fujian Normal University, Fuzhou, 350117, China*

[e] *Department of Oncology Surgery, General Hospital of Ningxia Medical University, Yinchuan, 750004, China*

[f] *Institute of Advanced Science Facilities, Shenzhen, Guangdong, 518107, China*

[g] *School of Biomedical Engineering, Guangzhou Medical University, Guangzhou, 511436, China*

[h] *School of Pharmaceutical Sciences and Institute of Materia Medica, Xinjiang University, Urumqi, 830017, China*

[i] *Yong Loo Lin School of Medicine and Faculty of Engineering, National University of Singapore, Singapore, 117597, Singapore*

A R T I C L E I N F O

Keywords:
Multimodal imaging
Ischemic stroke
Reperfusion injury
Carrier-free nanoagent
Ferroptosis

A B S T R A C T

Cerebral ischemia-reperfusion injury (CIRI) is a major challenge to neuronal survival in acute ischemic stroke (AIS). However, effective neuroprotective agents remain to be developed for the treatment of CIRI. In this work, we have developed an Anti-TRAIL protein-modified and indocyanine green (ICG)-responsive nanoagent (Anti-TRAIL-ICG) to target ischemic areas and then reduce CIRI and rescue the ischemic penumbra. *In vitro* and *in vivo* experiments have demonstrated that the carrier-free nanoagent can enhance drug transport across the blood-brain barrier (BBB) in stroke mice, exhibiting high targeting ability and good biocompatibility. Anti-TRAIL-ICG nanoagent played a better neuroprotective role by reducing apoptosis and ferroptosis, and significantly improved ischemia-reperfusion injury. Moreover, the multimodal imaging platform enables the dynamic *in vivo* examination of multiple morphofunctional information, so that the dynamic molecular events of nanoagent can be detected continuously and in real time for early treatment in transient middle cerebral artery occlusion (tMCAO) models. Furthermore, it has been found that Anti-TRAIL-ICG has great potential in the functional reconstruction of neurovascular networks through optical coherence tomography angiography (OCTA). Taken together, our work effectively alleviates CIRI after stoke by blocking multiple cell death pathways, which offers an innovative strategy for harnessing the apoptosis and ferroptosis against CIRI.

* Corresponding authors.
** Corresponding author.
*** Corresponding author.
**** Corresponding author. State Key Laboratory of Vaccines for Infectious Diseases, Xiang An Biomedicine Laboratory, Center for Molecular Imaging and Translational Medicine, Department of Vascular & Tumor Interventional Radiology, The First Affiliated Hospital of Xiamen University, School of Medicine, School of Public Health, Xiamen, 361102, China.
E-mail addresses: fanzhongxiong@xju.edu.cn (Z. Fan), Xiaofei5132004@163.com (X. Wen), maojingsong163@163.com (J. Mao), zhaoql@xmu.edu.cn (Q. Zhao).
[1] Q. Yang, W. Ye and D. L contributed equally to this work.

https://doi.org/10.1016/j.mtbio.2024.101094
Received 21 January 2024; Received in revised form 8 May 2024; Accepted 19 May 2024
Available online 22 May 2024

1. Introduction

Ischemic stroke, is the second leading cause of both death and disability worldwide [1,2]. The region of localized cerebral ischemia consists of the infarct core and the surrounding ischemic penumbra. Lethal ischemia and hypoxia occurred in the infarct core lead to neuronal necrosis, and the area of irreversible damage expands over time [3]. Brain cells in the ischemic penumbra only survive for a few hours, and the degree of neurological function damage worsens upon the increase of ischemic time. Once the blood supply to the ischemic penumbra is rapidly restored within a short time or other effective therapy methods are adopted, the brain injury is reversible, and it is possible for the nerve cells to survive and regain function [4,5]

Recently, the effectively therapeutic strategy of AIS mainly focus on rapid reperfusion with intravenous thrombolysis or endovascular thrombectomy [6], which are time-critical [7]. Intravenous thrombolysis has a narrow time window (used within 4.5 h of stroke onset) and is limited by contraindications [8], and mechanical thrombolysis is extremely limited in duration (generally no more than 8 h). Thrombectomy is also limited to large vessel occlusion [9–12].

However, cerebrovascular recanalization will trigger unavoidable reperfusion injury, leading to a series of harms such as oxidative stress, inflammatory response, and blood-brain barrier (BBB) damage [7]. It greatly affects the functional recovery and survival of brain nerve cells. A definitive solution has not been found for the control of reperfusion injury [13]. Cerebral ischemia-reperfusion injury should be actively prevented and treated in the clinic to reduce its harm to the brain. The treatment for cerebral ischemia-reperfusion injury may provide a new therapeutic basis and program for ischemic stroke.

Neuroprotective agents have the ability to reduce CIRI and can also be used as adjunctive therapies to revascularization, allowing brain cells to survive and stabilize the ischemic penumbra [14]. Although some developed neuroprotective agents (nerinetide [15], Neu2000 [16], and uric acid [17]) have shown an excellent therapeutic promise in clinical applications, their therapeutic efficacy is still unsatisfactory. This is mainly due to the delivery of neuroprotective agents across the BBB to poorly perfused brain tissue is inefficient. Even a compromised and more permeable BBB after a stroke can pose a serious challenge to drug delivery to the brain [18–20]. For many small molecule drugs, in addition to poor BBB-mediated accumulation in the central nervous system, their short half-life and rapid elimination from the circulation impair their absorption. In addition, limited antioxidant and anti-inflammatory activity and lack of specific targeting ability have contributed to the failure of some neuroprotective agents in clinical trials [21]. Therefore, explore an effective neuroprotective agent against ischemia-reperfusion injury will play an important role [22–24].

Tumor necrosis factor (TNF)-related apoptosis-inducing ligand (TRAIL), also known as Apo-2 ligand (Apo2L), is a member of the TNF cytokine superfamily. In conventional studies, it's a potent anticancer agent because it specifically targets cancer cells while sparing normal cells, and inducing cell apoptosis [25,26]. TRAIL can lead to direct activation of the caspase cascade resulting in apoptotic cell death [27]. TRAIL is also involved in cell apoptosis after focal cerebral ischemia, which appears to be mediated by activation of caspase-8 and caspase-3, as well as phosphorylation of the stress kinase JNK. TRAIL antibody has been shown to inhibit apoptosis in the penumbra region, thereby preventing infarct propagation [28]. Moreover, ferroptosis has been shown to have significant implications in ischemic injury [29]. Ferroptosis inhibition protected mice against ischemia-reperfusion injury, indicating that ferroptosis contributes to neuronal death after ischemic stroke [30]. It has been proved that there was a crosstalk between ferroptosis and apoptosis. Reactive oxygen species (ROS) were involved in both ferroptosis and TRAIL-induced apoptosis by upregulating DR4 and DR5 receptors [31–33]. The above studies show that TRAIL antibody may not only reduce neuronal apoptosis but also decrease neuronal ferroptosis, which could play a neuroprotective role. Therefore, TRAIL antibody may be more effective than other neuroprotective agents in reducing neuronal damage.

Numerous studies have shown that using of nanoparticles (NPs) formulations may improve drug transport across the BBB in ischemic disorders [20,34–36]. Compared to the traditional carrier based nanoscale drug delivery system, the carrier-free nanoagent has outstanding advantages including a simple preparation process and ultra-high drug loading capacity, while avoiding the side effects caused by carrier materials [37–39]. These increase the potential for clinical applications of the carrier-free nanoagent. In addition, indocyanine green (ICG) is widely used clinically as an aid in the diagnosis of liver function, cardiac output, and retinal vascular system [40,41]. ICG combined with drug molecules can be used for bimodal fluorescence (FL)/photoacoustic (PA) imaging to visualize drug entry into the brain in real time. This technique can help ensure an effective concentration of the drug in the injured brain region during personalized treatment, thus improving stroke treatment [42–44]. Moreover, combining MRI and OCTA provides a powerful method to assess neuronal damage during CIRI therapy [45].

Herein, we have developed a carrier-free nanoagent by combining a TRAIL antibody with ICG, which shows promise for the treatment of CIRI (Scheme 1). *In vitro* cellular experiments and *in vivo* therapeutic studies have shown that the Anti-TRAIL-ICG nanoagent exhibited desirable effects in treating CIRI, by suppressing neuronal apoptosis and ferroptosis. Additionally, the paracellular permeability of the BBB is significantly increased in acute ischemic stroke due to impaired tight junctions. This can further enhance the delivery of nanoparticles to the infarcted area of brain and provide neuroprotection against CIRI. Furthermore, in combination with multi-modal imaging technology, our research has achieved comprehensive and accurate visual efficacy monitoring of ischemia-reperfusion areas. This provides a theoretical basis and new ideas for innovative optimization of clinical treatment of ischemic stroke.

2. Results and discussion

Synthesis and Characterization of Anti-TRAIL-ICG nanoagent. The activated ester of the succinimide lipids (NHS) can react rapidly and be linked with the primary amine (-NH_2) on the antibody with high specificity, thus coupling the ICG to the antibody. The one-step preparation process of the Anti-TRAIL-ICG nanoagent is shown in Fig. 1A. After mixing and ultrafiltration procedures, the ICG-loaded TRAIL antibody was obtained. Transmission electron microscope (TEM) images indicated that the nanoagent have a spherical morphology with a particle size around 100 nm (Fig. 1B). Dynamic light scattering (DLS) measurement further confirmed that the hydrodynamic size of Anti-TRAIL combined with ICG is around 100 nm (Fig. 1C). As shown in Fig. 1D, the change in surface charge indirectly demonstrated the effective loading of TRAIL antibody on ICG. Compared to the nanomaterials with positively charged surface, the synthesized Anti-TRAIL-ICG nanoparticles with negatively charged surface have less toxicity [46]. Their charged surface was less than −30 mv or 30 mv, which also maintains interparticle repulsion and stable particle suspension.

The absorption and fluorescence spectral characteristics of the fluorescent marker can change when coupled to a protein such as an antibody [43]. Therefore, we measured the absorption and fluorescence spectra of the Anti-TRAIL-ICG. Fig. 1E and F showed that the labelled antibody was successfully excited and fluoresced with a spectral pattern similar to that of ICG, confirming that the labelled antibody retains the fluorescence characteristics of the ICG dye [43]. The absorbance of Anti-TRAIL-ICG in water, PBS, Fetal bovine serum (FBS), and DMEM was measured on days 1, 3, and 5. The absorbance and color of the solution did not change significantly, indicating its good physical stability (Fig. 1G and H). The ICG loading efficiency was further measured to be 25.76 % ± 0.11 % (Table S1). Oxygen and glucose deprivation/reperfusion (OGD/R) cells have been extensively applied as *in vitro*

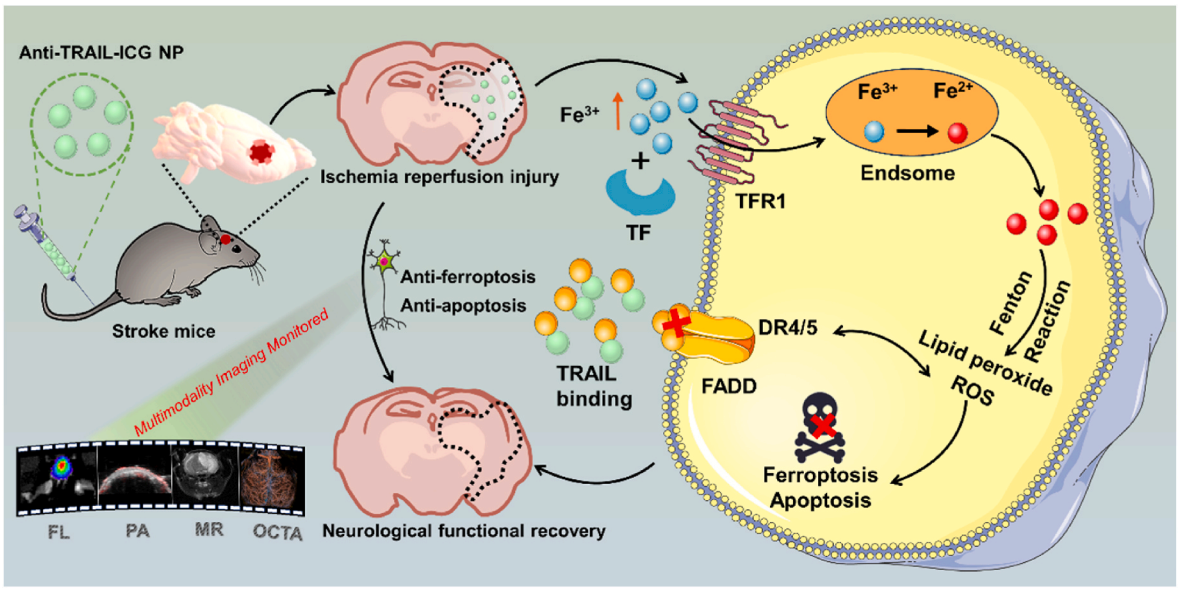

Scheme 1. Anti-TRAIL-ICG nanoagent exerts Anti-ferroptosis and Anti-apoptosis effects synergistically to reduce ischemia-reperfusion injury after stroke, and multimodal optical imaging were used for better precision therapy. TF: Transferrin.

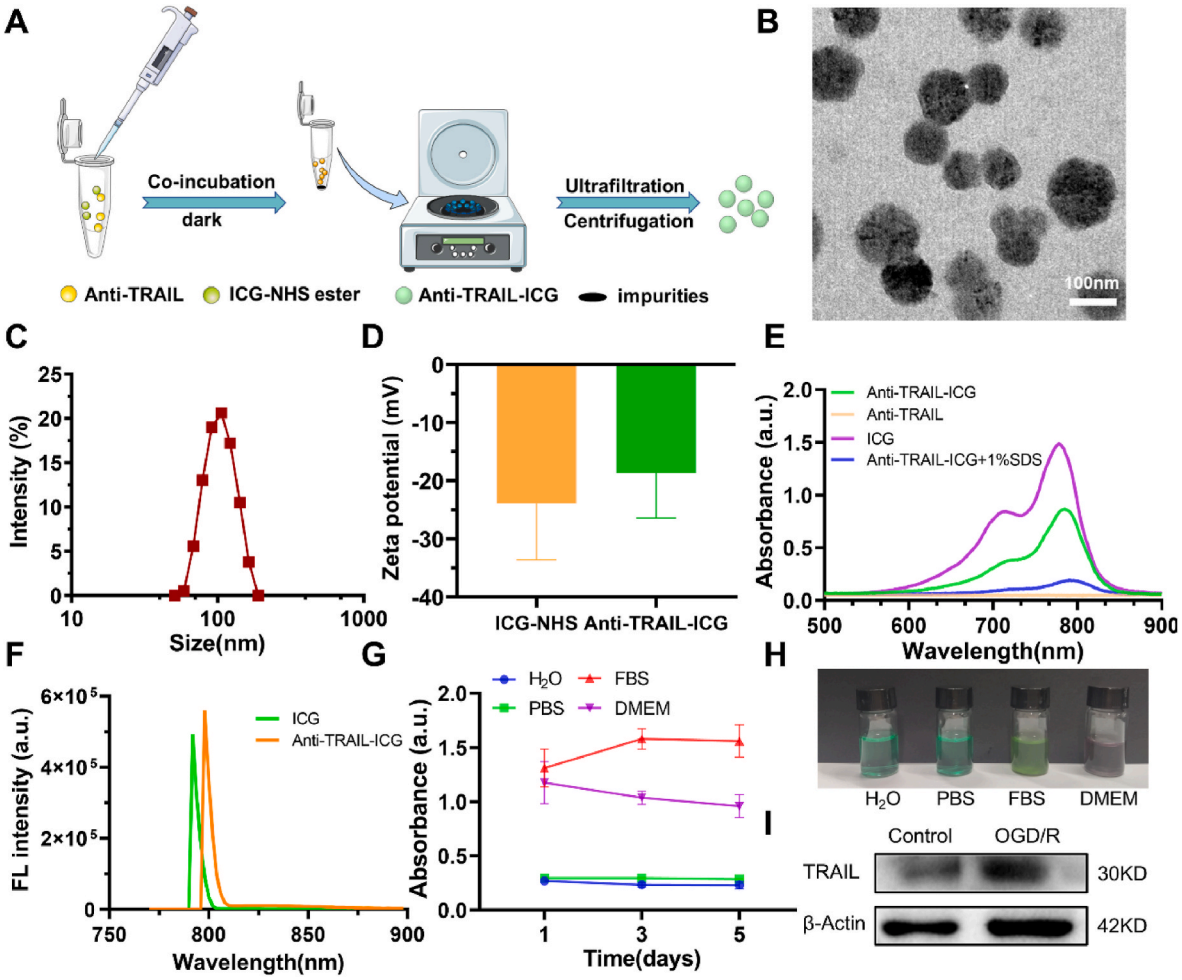

Fig. 1. Synthesis and characterization of Anti-TRAIL-ICG nanoagent. (A) The schematic diagram of the preparation process of Anti-TRAIL-ICG nanoagent. (B) TEM images of Anti-TRAIL-ICG. (C)Intensity of Anti-TRAIL-ICG by DLS measurement. (D) Zeta potential of ICG-NHS and Anti-TRAIL-ICG. (E) Absorbance spectra of the TRAIL antibody, ICG, the Anti-TRAIL-ICG, and Anti-TRAIL-ICG conjugate in 1 % SDS. (F)Fluorescence spectra of ICG and Anti-TRAIL-ICG. (G) Absorbance changes of Anti-TRAIL-ICG nanoagent dissolved in water, PBS, FBS, and DMEM on days 1, 3, and 5. (H) White light plots of Anti-TRAIL-ICG nanoagent in different solutions on days 5. (I) Identification of Anti-TRAIL-ICG nanoagent combined with TRAIL by Western blot (WB).

models in stroke-relevant studies [47]. TRAIL expression was upregulated in N2a cells treated with OGD/R. The Western blot results in Fig. 1I showed that Anti-TRAIL-ICG still has a good binding capacity to the TRAIL antigen.

***In vitro* active targeting ability of Anti-TRAIL-ICG.** TRAIL is a 281-amino acid type II transmembrane protein that belongs to the TNF superfamily [48]. It's an innate immune cytokine widely expressed on immune cells including lymphocytes, natural killer cells, and neutrophils [49]. After cerebral ischemia, TRAIL expression was upregulated and released from glial cells and injured neurons, triggering neuronal apoptosis [50,51]. To validate the targeting ability of Anti-TRAIL-ICG, the expression level of TRAIL was observed in OGD/R treated N2a cells. First, we investigated the expression status of TRAIL protein in N2a cells after OGD with different reoxygenation and reglucose times (Fig. S1). Western blot results showed a significant increase in TRAIL protein at 24 h after OGD/R (Fig. 2A and B), verifying that TRAIL could be a therapeutic target for CIRI.

The cellular uptake of Anti-TRAIL-ICG was then investigated by confocal fluorescence microscopy. The Anti-TRAIL-ICG treated group showed high red fluorescence intensity compared with the rest groups (Fig. 2C). Flow cytometry analysis showed that N2a cells decreased the uptake of free ICG after OGD/R, whereas the uptake of Anti-TRAIL-ICG was not significantly affected (Fig. 2D–S2). These results indicated that Anti-TRAIL-ICG has excellent active targeting, which is beneficial for therapy of ischemia reperfusion injury.

***In vitro* neuroprotective effects of Anti-TRAIL-ICG.** To evaluate the protective effect of Anti-TRAIL-ICG on neuronal cells, we investigated whether Anti-TRAIL-ICG could reduce apoptosis and ferroptosis of N2a cells after OGD/R. PI/Hoechst staining showed that cell apoptosis and necrosis were significantly reduced in the Anti-TRAIL-ICG (20 μg/mL) treated group compared to the OGD/R group (Fig. 3A). Flow cytometric analysis also showed protective effect of Anti-TRAIL-ICG on N2a cells after OGD/R (Fig. 3B). We subsequently evaluated the levels of ROS and LPO, which could cause cell ferroptosis. 2′,7′-dichlorofluorescin diacetate (DCF-DA) is a probe that can penetrate cells and be used to detect the production of ROS within cells. The results of immunofluorescence and flow cytometry analysis of DCF-DA indicated that Anti-TRAIL-ICG could significantly reduce ROS levels in OGD/R treated N2a cells. (Fig. 3C and D). Disruption of lipid membranes is a prominent feature of ferroptosis. And LPO levels were consistent the trend of ROS measurements (Fig. 3E). Notably, although very limited, the ICG group seemed to reduce the levels of ROS and LPO in OGD/R-treated N2a cells. This may be due to the fact that the sulfonate in free ICG complexes with Fe^{3+}, thereby inhibiting the iron metabolism pathway in activated N2a cells and attenuating cellular ferroptosis [52,53]. Finally, cell viability was determined using the CCK8 assay. As shown in Fig. S3, Anti-TRAIL-ICG was able to increase the cell viability of N2a cells after OGD/R, but had no effect on normal cells. Thus, Anti-TRAIL-ICG exert an excellent neuroprotective effect on ischemic injury by effectively reducing apoptosis and suppressing the intracellular production of classical indicators of ferroptosis (ROS and LPO) [54].

***In vivo* photoacoustic (PA) and fluorescence (FL) imaging.** First, we established transient middle cerebral artery occlusion (tMCAO) stroke model in mice. Achievement of ischemia was confirmed by

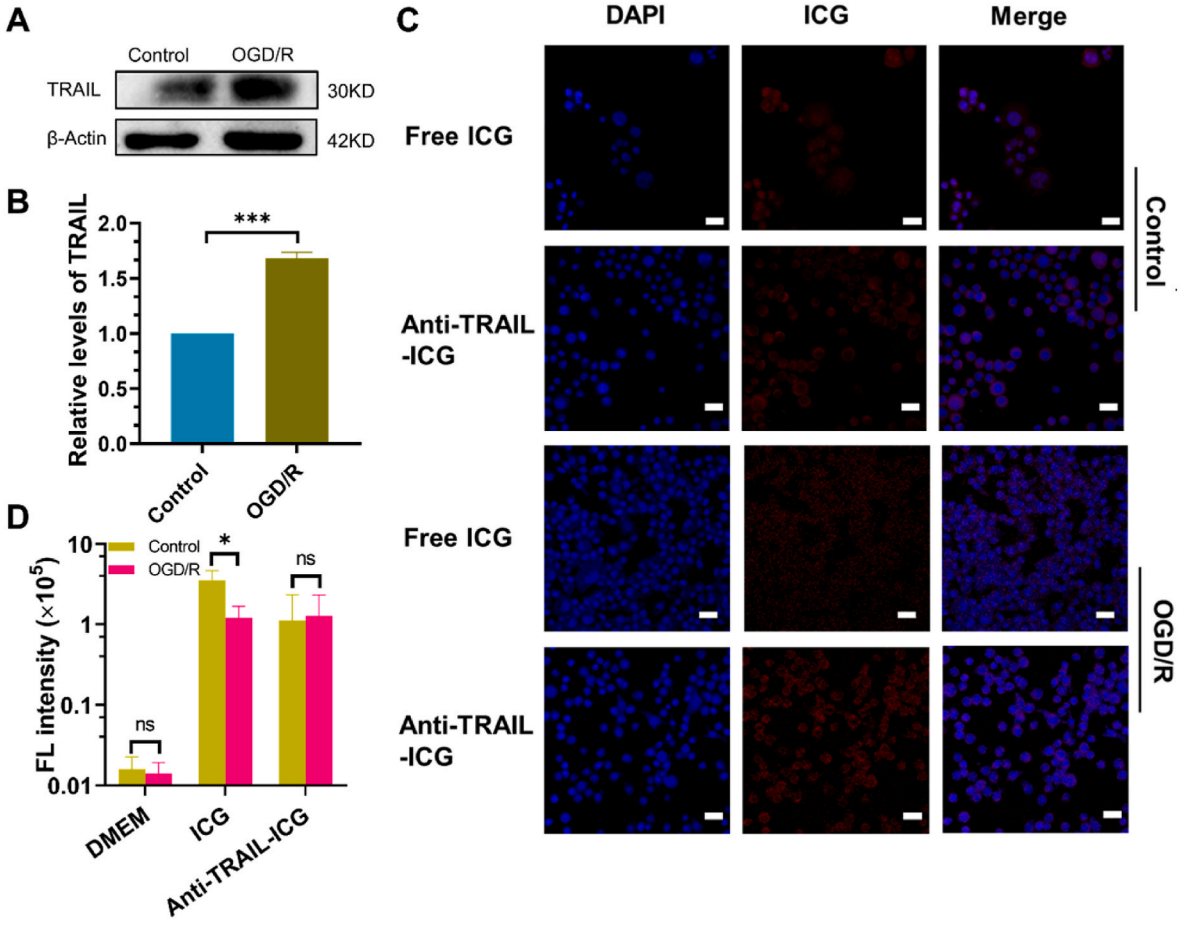

Fig. 2. *In vitro* active targeting ability of Anti-TRAIL-ICG. (A) Relative expression of TRAIL in the N2a cells after 24 h OGD/R. (B) Quantitative analysis of TRAIL protein after 24 h OGD/R. n = 3 (C) Subcellular localization of ICG in N2a cells after incubation with free ICG or Anti-TRAIL-ICG for 4 h. (D) Quantitative analysis of the mean fluorescence intensities of free ICG and Anti-TRAIL-ICG in OGD/R-activated N2a cells and normal N2a cells. Scale bar:30 μm. n = 3 $^{*}p < 0.05$, $^{**}p < 0.01$, $^{***}p < 0.001$.

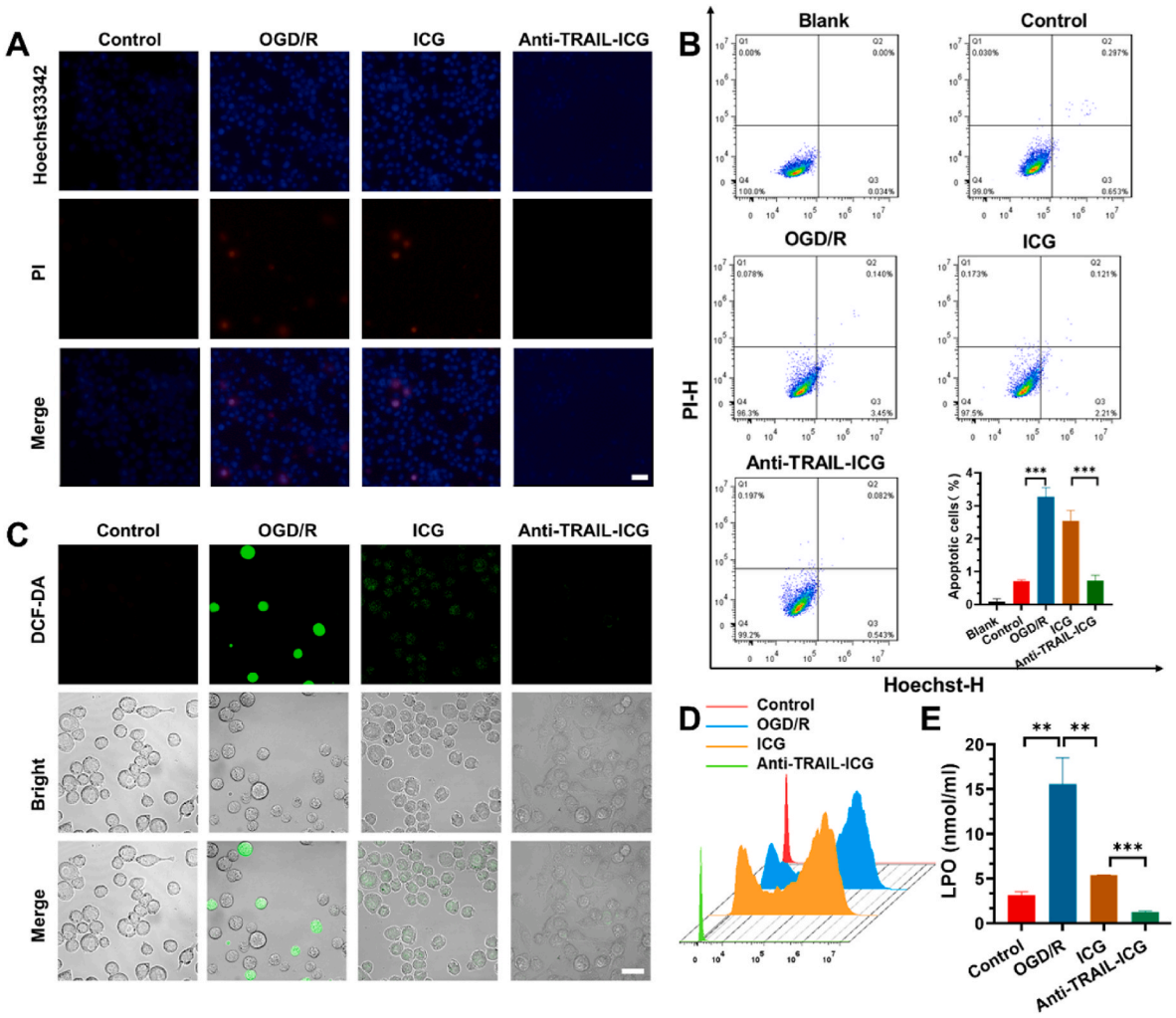

Fig. 3. ***In vitro*** **neuroprotective effects of Anti-TRAIL-ICG.** (A) Representative images of PI/Hoechst33342 staining of N2a cells in different groups after OGD/R; Scale bar: 50 μm. (B) Representative images of cell apoptosis analyzed by Flow cytometry, where N2a cells were incubated with different formulations after OGD/R. (C) Representative images of intracellular ROS levels in different groups; Scale bar: 30 μm. (D) Flow cytometric curve of DCF-DA fluorescence intensity in various groups. (E) Expression level of LPO in various groups. *p < 0.05, **p < 0.01, ***p < 0.001.

monitoring regional cerebral blood flow through laser speckle contrast imaging (Figs. S4A and B). Animals without a reduction of at least 80 % cerebral blood flow were excluded from the study (Fig. S4C). The successful establishment of the murine tMCAO model was then confirmed by TTC staining [55] (Fig. S4D).

To verify the targeting ability of Anti-TRAIL-ICG *in vivo*, dual-modal imaging was performed in mice after tMCAO. Free ICG and Anti-TRAIL-ICG (1 mg/kg, *i. v.*) were administered simultaneously with reperfusion. As shown in Fig. 4A, both free ICG and Anti-TRAIL-ICG were distributed in the brain, which may due to BBB damage after cerebral ischemia and reperfusion might account for this. Compared with the ICG-treated group, the fluorescence signal was stronger in the Anti-TRAIL-ICG-treated group, which reached a maximum FL accumulation at 4 h post-injection. Quantitative analysis of the FL signal in the Anti-TRAIL-ICG-treated group was nearly 9-fold higher than that in the free ICG-treated group at 4 h post-injection, demonstrating the superior brain-targeting ability of Anti-TRAIL-ICG *in vivo* (Fig. 4B). Notably, the signal intensity didn't significantly decrease at 24 h post-injection, indicating that Anti-TRAIL-ICG can provide long-term protection against ischemic stroke. Anti-TRAIL-ICG exhibited a longer blood retention time. The *in vivo* fluorescence images were consistent with the above phenomenon (Fig. 4C and D). These result agree with the previous finding that NPs of 50–100 nm in diameter are desirable for transport across the BBB [56]. In addition to this, there was a weak nanoagent signal in the brain of normal mice, whereas the nanoagent signal was strong in the brain of ischemia-reperfusion mice (Fig. S5). The ability of Anti-TRAIL-ICG nanoagent to differentiate normal mice from stroke mice suggests its diagnostic potential.

The *in vivo* PA imaging could provide excellent resolution and high contrast for biological tissues [57]. Similar to FL imaging, Anti-TRAIL-ICG showed high signal in PA imaging (Fig. 4E and F). This suggested that Anti-TRAIL-ICG nanoagent as a bimodal contrast agent, also have a remarkable property of PA imaging. And this facilitated the observation of Anti-TRAIL-ICG distribution in brain regions. In conclusion , Anti-TRAIL-ICG could enhance the accumulation of Anti-TRAIL in the brain of mice after acute ischemic stroke due to the excellent targeting ability. And it was a promising therapeutic target for ischemic stroke.

Real-time monitoring of drug infiltration indeed plays a substantial role in the treatment of diseases, particularly when it comes to managing complex conditions such as CIRI following AIS. Through real-time monitoring, doctors can accurately understand the distribution and concentration changes of drugs in the lesion area, which is crucial to ensure that the drugs effectively reach the lesion site and maintain the concentration required for treatment [58,59].

Anti-TRAIL-ICG protected against CIRI in mice. Based on *in vitro*

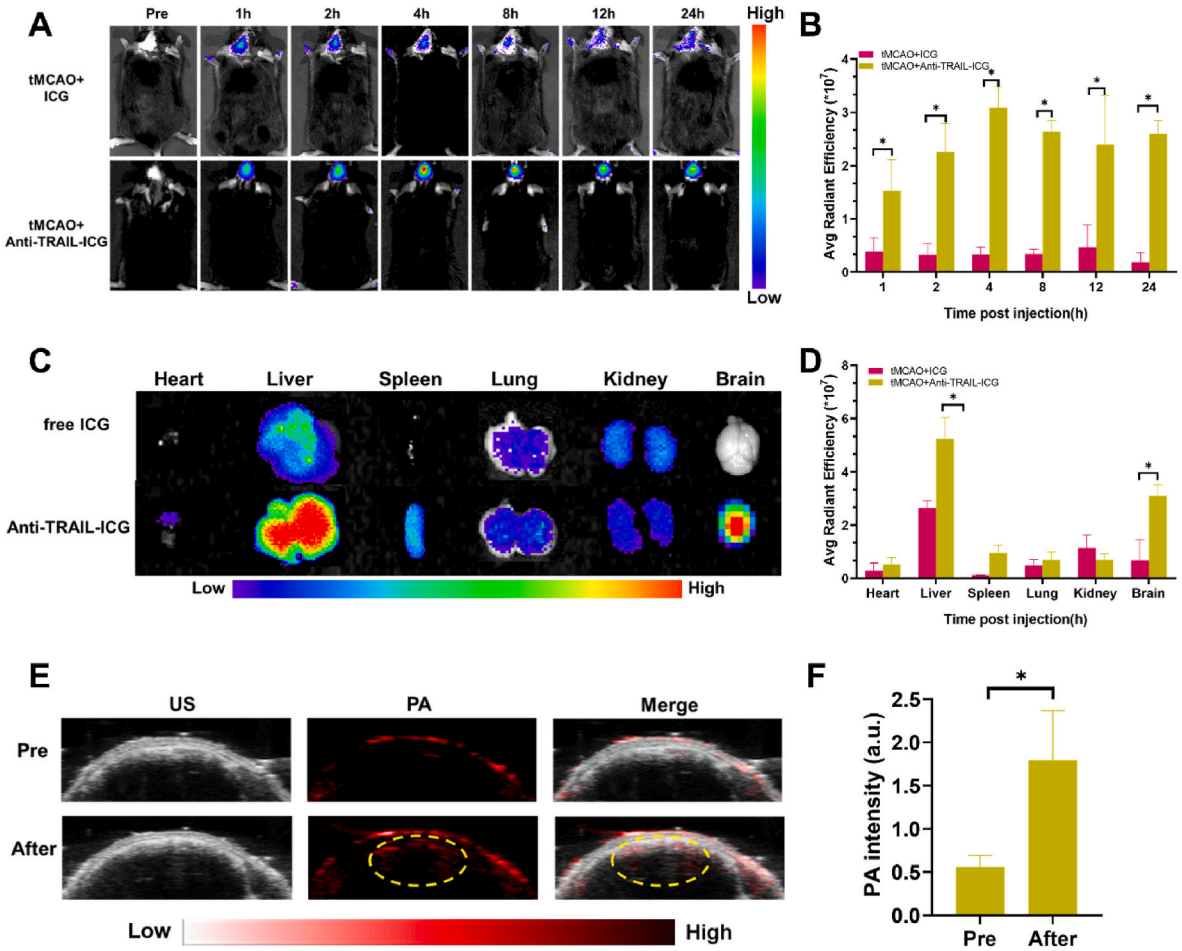

Fig. 4. ***In vivo*** **photoacoustic (PA) and fluorescence imaging.** (A) Fluorescence imaging of ICG and Anti-TRAIL-ICG (1 mg/kg, *i. v.*) accumulated in tMCAO mice at different time points. (B) Quantitative analysis of fluorescence intensity of brain at different time points (n = 3). (C) Quantitative analysis of fluorescence intensity of major organs *in vitro* (n = 3). (D) Fluorescence imaging of major organs *in vitro* at 4 h after administration of ICG and Anti-TRAIL-ICG. (E) PA imaging of tMCAO mice pre-and post-Anti-TRAIL-ICG injection. (F) Quantitative analysis of PA signal strength in tMCAO mice. $^{*}p < 0.05$, $^{**}p < 0.01$, $^{***}p < 0.001$.

results, the efficacy of Anti-TRAIL-ICG was evaluated in tMCAO mice. Mice were randomly divided into three groups after a 0.5 h occlusion, mice were intravenously injected with vehicle (tMCAO), 1 mg/kg ICG (tMCAO + ICG), 1 mg/kg Anti-TRAIL-ICG (tMCAO + Anti-TRAIL-ICG) with reperfusion. Fig. 5A showed the schematic diagram of the experiments in mice. Compared to the vehicle and ICG group, Anti-TRAIL-ICG (1 mg/kg, *i.v.*) significantly reduced the neurological deficit score and 7-day survival rate, and reversed the weight loss (Fig. 5B–D).

Furthermore, we evaluated the efficacy of nanoagent in protecting ischemic penumbra. The MRI T_2-weighted images showed that the Anti-TRAIL-ICG group significantly reduced the cortical infarct area compared to the vehicle and ICG group, particularly at the level of the striatum and hippocampus (Fig. 5E and F). This reduction of the brain infarction was associated with improvement of the neurological scores in mice [60]. In all, a single administration of Anti-TRAIL-ICG (1 mg/kg, *i. v.*) at the same time as reperfusion exerted a neuroprotective effect against CIRI in mice.

Anti-TRAIL-ICG reduced neuronal cell death and accelerated the functional reconstruction of neurovascular network. To elucidate the mechanism of Anti-TRAIL-ICG against cerebral ischemic injury, we performed the following investigations. First, the staining of Nissl bodies in normal cells is uniform. However, the nucleus was shrunken, the color was darker, and the size and number of Nissl bodies became smaller in the infarct area due to cell necrosis. Administration of Anti-TRAIL-ICG significantly improved those changes. The results of Nissl staining also showed that the infarct area was significantly reduced in the Anti-TRAIL-ICG group than in the vehicle group, indicating that the ischemic penumbra could be effectively rescued (Fig. 6A). We then tested whether Anti-TRAIL-ICG could alleviate neuronal ferroptosis. We observed that GPX4 was upregulated in the ischemic penumbra (Fig. 6B), and we speculated that neurons in this region increased GPX4 in order to antagonize ferroptosis. Subsequently, we found that the expression of MDA was up-regulated after stroke, and administration of Anti-TRAIL-ICG could reduce the level of MDA (Fig. 6C). This proved that ferroptosis occurred in neuronal cells after ischemic stroke and Anti-TRAIL-ICG could rescue brain injury by alleviating ferroptosis.

Neurogenesis and neovascularization have been shown to promote the restoration of the blood-brain barrier [61]. Neural repair and functional restroation requires consideration of neovascularization after stroke. The natural repair process after cerebral ischemia was accompanied by neurogenesis and neovascularization, however, this spontaneous stress repair process was weak and insufficient to restore neurovascular homeostasis after brain injury [62]. Remodeling of the neurovascular network requires the administration of exogenous or other drugs to rescue brain damage and improve neurological dysfunction. We wondered whether Anti-TRAIL-ICG could affect neurovascular network remodeling. Overall changes in cerebral microvascular morphology and angiogenesis can be well monitored and evaluated using OCTA [63–66]. We therefore used OCTA to monitor angiogenesis in mice at 7 days after tMCAO. We selected the cortical branch of the right middle cerebral artery in mice for observation, and compared vascular injury in different groups of mice before stroke with that 7 days

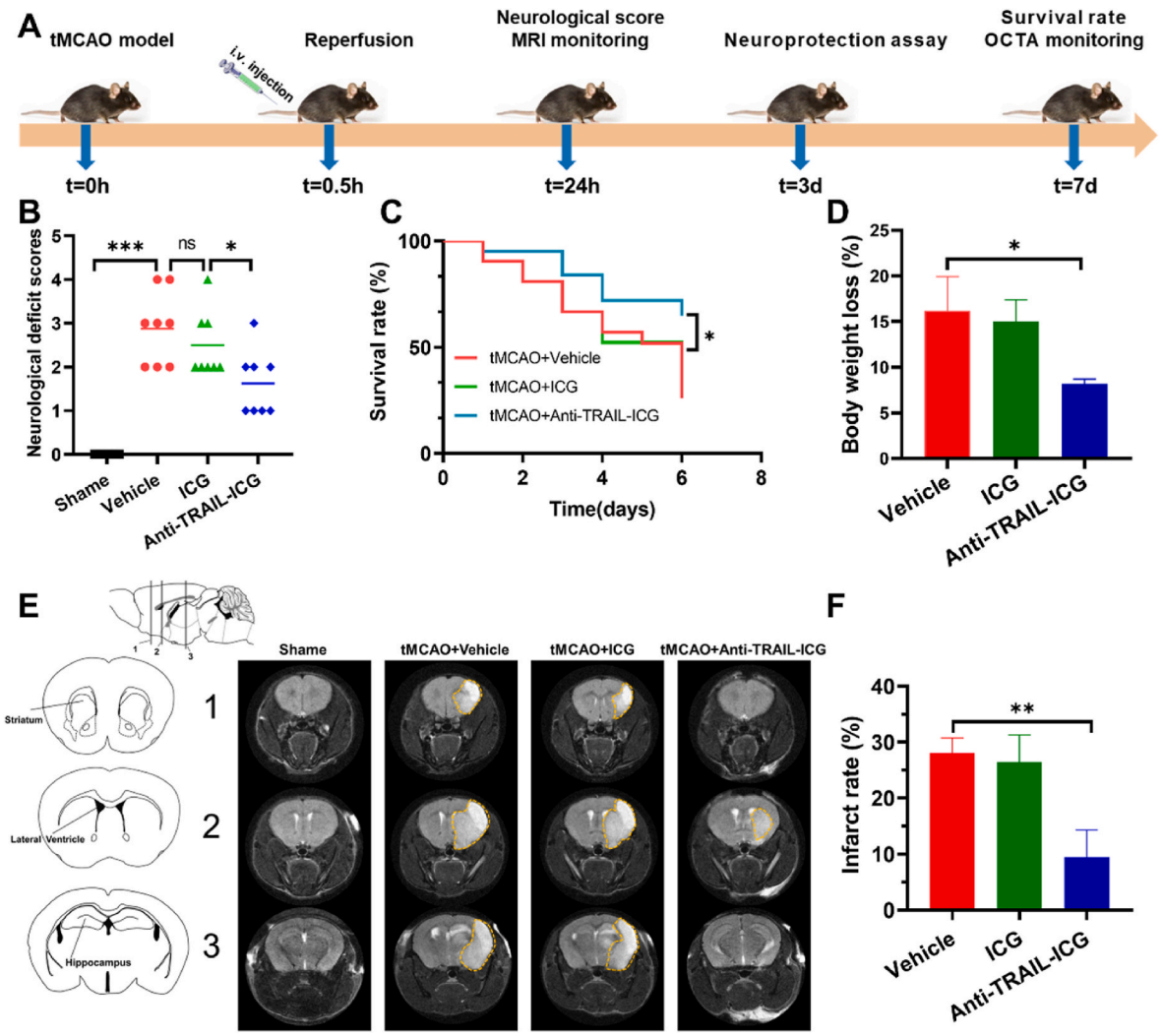

Fig. 5. Anti-TRAIL-ICG protected against CIRI in mice. (A) The schematic diagram of the *in vivo* experiments. (B) Neurological deficit score was determined at 24 h after stroke (n = 8). (C) Survival curve after 7 days in different groups. (D) Percentage of weight loss at 24 h after tMCAO (n = 3). (E) Representative T2-weighted MRI images at striatal, lateral ventricular and hippocampal levels. (F) Quantification of cerebral infarct volume (n = 3). $^{*}p < 0.05$, $^{**}p < 0.01$, $^{***}p < 0.001$.

after stroke. As shown in Fig. 6D, the cerebral cortex microvessels were destroyed after stroke. Compared with the ICG-treated group, the Anti-TRAIL-ICG-treated group effectively promoted cerebral microvascular neovascularization, indicating that it promoted the remodeling of neurovascular homeostasis after stroke. The mechanism of its effect on revascularization needs to be further explored. In order to quantify the vascular information captured by OCTA, we first implemented the initial segmentation of microvessels using MATLAB [67] (Fig. S6). Subsequently, the microvascular information of each group was analyzed using Vessels percentage area, Average Vessels Length, Junctions density, and Mean E Lacunarity as the main assessment objectives. Vessels percentage area, average vessels length, and junction's density are positively correlated with the proportion of neovascularization. Compared to the tMCAO and the ICG groups, the Anti-TRAIL-ICG-treated group had a higher proportion of neovascularization and was closest to the cerebral vasculature of normal mice (Figs. S7A–C). Mean E Lacunarity (Fig. S7D), on the other hand, had the opposite trend of the above indicators, indirectly confirming the reliability of the above results. These results demonstrated that Anti-TRAIL-ICG can reduce neuronal cell death and accelerate the functional recovery of the neurovascular network, suggesting that it has the potential as an effective drug for the treatment of ischemic stroke in future. Further research is underway to determine how the Anti-TRAIL-ICG nanoagent regulates both apoptosis and ferroptosis mechanisms simultaneously, as well as its effect on the remodeling of the neurovascular network.

***In vitro* and *in vivo* biosafety and compatibility assessment.** The biosafety of Anti-TRAIL-ICG was assessed by cytotoxicity, hemolysis assay and H&E stained histological analysis. The cell viability of N2a and bEnd.3 cells was maintained at a high level with the increasing concentration of Anti-TRAIL-ICG, indicating that Anti-TRAIL-ICG is a less toxic drug (Fig. 7A and B). The hemolysis rate was less than 5 %, indicating good biosafety (Fig. 7C). Moreover, no significant tissue damage was observed in the tissues of the ICG group and Anti-TRAIL-ICG group, indicating that the carrier-free theranostic nanoagent possessed excellent safety and compatibility, and would not activate any inflammation or immune response (Fig. 7D).

3. Conclusion

In conclusion, we have successfully developed a carrier-free Anti-TRAIL-ICG nano-preparation to reduce ischemia reperfusion injury and rescue ischemic penumbra. The preparation process is convenient and safe, and the resulting carrier-free nanomedicines are less toxic. Besides, *in vitro* results show that the Anti-TRAIL-ICG effectively inhibited apoptosis and ferroptosis in cells associated with OGD/R after

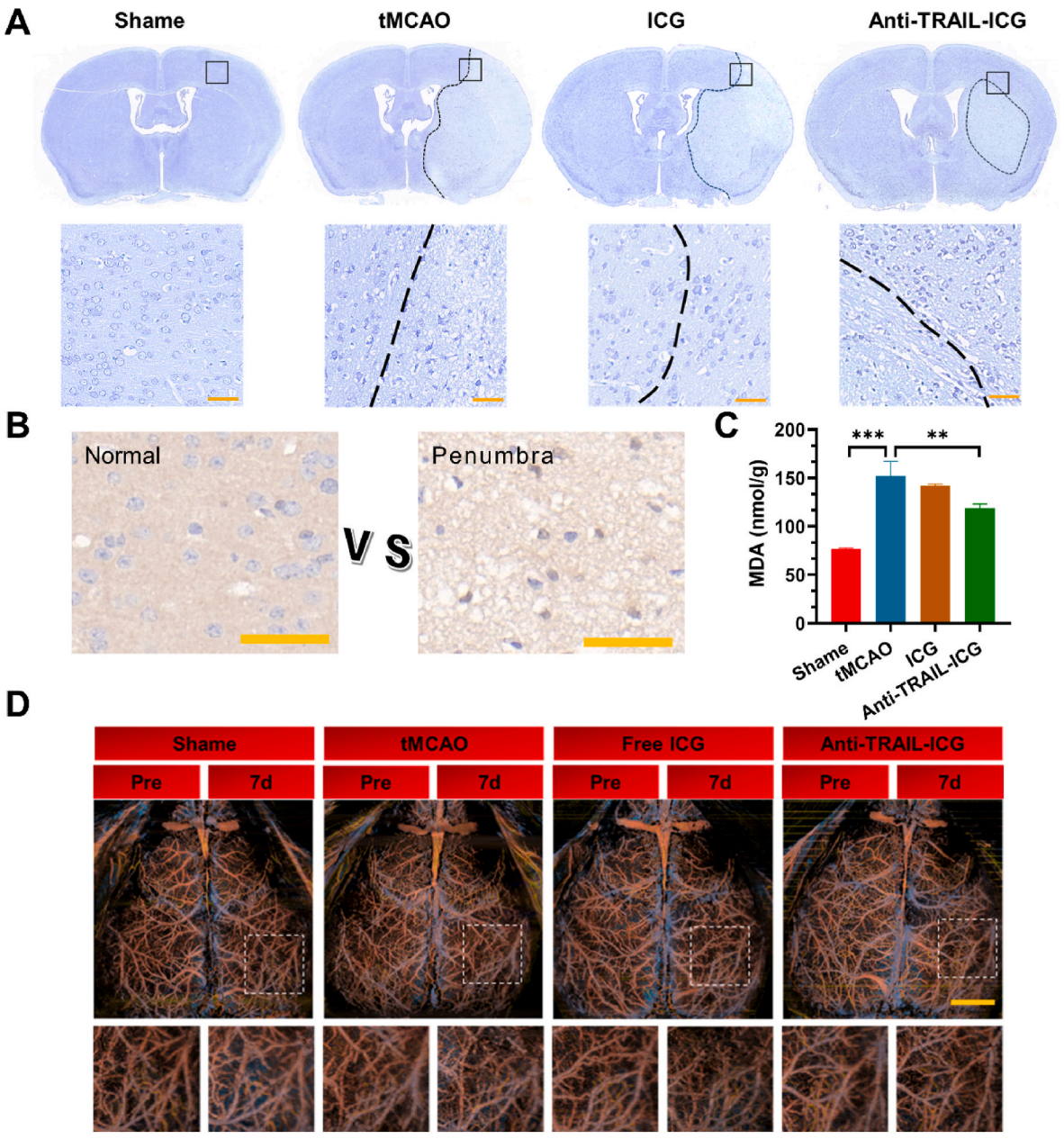

Fig. 6. Anti-TRAIL-ICG reduced neuronal cell death and accelerated the functional reconstruction of the neurovascular network. (A) Effect of Anti-TRAIL-ICG on cortex neuronal damage evaluated by Nissl staining. Scale bar: 50 μm (B) Representative immunohistochemistry (IHC) images of GPX4 in normal and penumbra regions; Scale bar: 50 μm. (C) MDA expression of brain tissue in different groups. (D) OCT angiographic images of cortical branches of the middle cerebral artery in different groups of mice. Scale bar: 2 mm $^{*}P < 0.05$, $^{**}P < 0.01$, $^{***}P < 0.001$.

intracellular uptake. In addition, Anti-TRAIL-ICG showed significant accumulation in the cerebral ischemic tissue of mice with induced ischemic stroke after *i. v.* administration. *In vivo* results demonstrated that the Anti-TRAIL-ICG can be considered as an effective neuroprotective drug in IS, especially its potential in the functional reconstruction of the neurovascular network. Therefore, this study used ICG as the imaging molecule and TRAIL antibody as the functional core to target ischemic neurons in the brain and inhibit ferroptosis and apoptosis may achieve satisfactory therapeutic effect in the neuroprotective treatment of stroke. Taken together, our study proposes an Anti-TRAIL-ICG nanoagent, which can be further developed as promising multifunctional drugs for precision treatment of cerebral ischemia reperfusion injury.

4. Materials and methods

Preparation of Anti-TRAIL-ICG nanoagent. First, TRAIL antibody (Affinity) and ICG-NHS (Shaanxi Xinyan Bomei Biotechnology, China) were dissolved in dimethyl sulfoxide (DMSO) and incubated in distilled water in the dark for 24 h. Then, the mixture was ultrafiltered at 10000 rpm for 15 min. The ultrafiltration tubes have a molecular weight cutoff of 10 KD, and antibodies with molecular weights greater than 10 KD are retained. After two more ultrafiltration washes, ICG and other impurities with molecular weights much smaller than 10 KD are removed. Finally, Anti-TRAIL-ICG nanoagent was obtained by washing twice with distilled water.

Characterization of Anti-TRAIL-ICG nanoagent. The morphology of the Anti-TRAIL-ICG nanoagent was observed by Tecnai Spirit TEM. The effective nanoparticle diameters and surface charge of Anti-TRAIL-

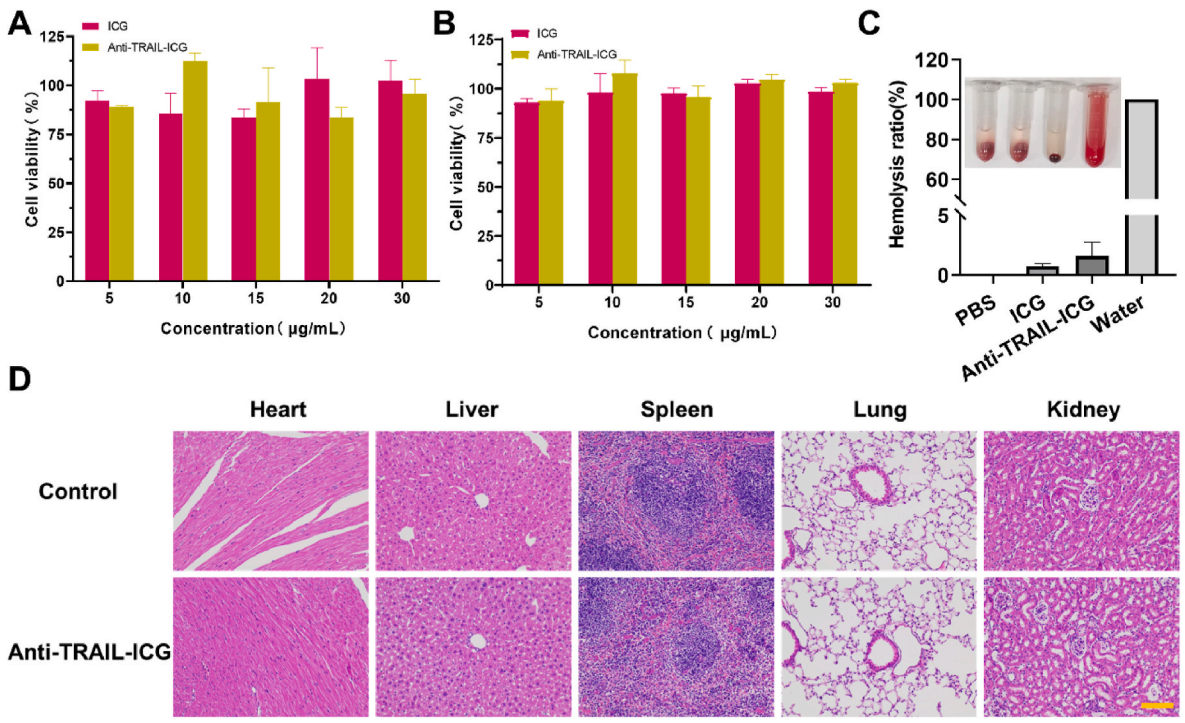

Fig. 7. *In* vitro and *in vivo* biosafety and compatibility assessment. (A) Cytotoxicity of ICG and Anti-TRAIL-ICG at different concentrations in N2a cells. (B) Cytotoxicity of ICG and Anti-TRAIL-ICG at different concentrations in bEnd.3 cells. (C) Hemolytic test. (D) Histological images of major organs after treatment with free ICG and Anti-TRAIL-ICG. Scale bar: 100 mm.

ICG nanoagent was determined by using DLS (Nanosizer, Malvern Instrument) at room temperature. Their absorption and fluorescence spectra were examined using a Tecan Spark multifunctional enzyme marker. WB assay was performed to characterize the ability of Anti-TRAIL-ICG to bind TRAIL using Anti-TRAIL-ICG as the primary antibody. The physical stability of Anti-TRAIL-ICG was evaluated by measuring its absorbance changes while dissolved in water, PBS, FBS, and DMEM (Gibco) on days 1, 3, and 5, respectively, using an enzyme marker (Tecan spark, Swizerland). 1 mg/mL of ICG-NHS was diluted into different concentrations by gradient dilution, after which its absorbance at 780 nm was measured by an enzyme marker. A standard curve was made based on the absorbance, and the concentration of ICG-NHS in the samples was calculated from the standard curve. ICG loading capacity = (mass of ICG-NHS in nanoparticles)/(total amount of Anti-TRAIL and ICG).

Cell cultures. Mouse N2a cells and bEnd.3 cells were cultured in DMEM medium containing 1 % penicillin-streptomycin (v/v) and 10 % (v/v) FBS at 37 °C under in a humidified atmosphere containing 5 % CO_2.

Cytotoxicity of free ICG and Anti-TRAIL-ICG nanoagent**.** N2a cells and bEnd.3 cells were seeded and cultured for 24 h in a 96-well plate (10^4 cells/well). The cells were then incubated with different doses in either free ICG form or TRAIL-ICG nanoagent for 4 h. After that, adding the CCK-8 was then added and incubated for the appropriate time. Finally, a multifunctional microplate reader was utilized to detect the absorbance of the solution in each well at 450 nm. There were three replicates in each group.

Establishment of an *in vitro* OGD/R model. The original culture solution was aspirated and washed three times with PBS buffer solutions. Glucose-free DMEM medium was added to the N2a cells, placed in an anoxic chamber (Aipuins) and exposed to a gas mixture of 95 % N2 and 5 % CO_2 for 2 h. The cells were then transferred to the original medium and incubated for 24 h under normal conditions.

Expression levels of TRAIL in OGD/R-treated N2a cells. OGD/R-treated N2a cells at different time points were lysed to release the target proteins. The protein concentration of the supernatant was determined by the BSA method. Equal amounts of protein were subjected to sodium dodecyl sulfate-polyacrylamide gel electrophoresis on 8 % and 12 % gels and then transferred onto Hybond ECL nitrocellulose membranes. The membranes were blocked with 5 % milk in PBST and then incubated overnight at 4 °C with a rabbit anti-TRAIL polyclonal antibody. After incubation with HRP-conjugated secondary antibody, detection was performed by means of ECL chemiluminescence assay. β-Tubulin (Acmec) was used as an internal control.

***In vitro* active targeting ability of Anti-TRAIL-ICG.** N2a cells were cultured for 24 h in confocal dishes (2×10^4 cells/well) with 1 mL growth medium. After changing to serum-free medium with or without OGD for 2 h, the cells were incubated with Anti-TRAIL-ICG or free ICG for 4 h. Then, washed three times with PBS buffer solutions. The samples were then fixed with 2 mL of 4 % paraformaldehyde (PFA) for 15 min. Finally, nuclei were stained with DAPI and imaged by laser scanning confocal fluorescence microscopy (Olympus FV1200, Japan). For the determination of cellular uptake, the N2a cells (2×10^4 cells/well) were seeded in 6-well plates and cultured with 20 μg/mL of either Anti-TRAIL-ICG or free ICG form. After incubation for 4 h, rinsed, the cells were rinsed, trypsinized and resuspended, and the ICG uptake was analyzed quantitatively using a cytometer (Beckman Cytoflex LX, USA).

Cellular apoptosis assay. N2a cells were plated on a 6-well plate (1×10^5 cells/well) and cultured for 24 h. Then, OGD was performed with serum-free medium for 2 h, transferred to normal medium with Anti-TRAIL-ICG or free ICG (20 μg/mL) for 24 h. And the apoptosis induced by OGD/R was examined through the Hoechst33342/PI assay (Solarbio, China). The N2a cells were examined under an inverted fluorescence microscope (Nikon Ti–U, Japan). Finally, fluorescence was quantified by flow cytometry.

Measurement of intracellular ROS generation. N2a cells were cultured separately in confocal dishes (2×10^4 cells/well) with 1 mL growth medium for 24 h. OGD was then performed with serum-free medium for 2 h, followed by transfer to normal medium with Anti-TRAIL-ICG or free ICG (20 μg/mL) for 24 h. Intracellular ROS levels

were then detected with DCF-DA (a fluorescent probe) using a commercially available kit (Solarbio). Specifically, cells were incubated with 10 μM DCF-DA at 37 °C for 20 min, and the fluorescence of DCF (deacetylated product of DCF-DA) was observed by confocal microscopy and quantified at 525 nm after excitation at 488 nm.

Measurement of intracellular LPO expression. As mentioned above, N2a cells were collected in centrifuge tubes and the supernatant were discarded after centrifugation. The expression level of LPO in different groups was measured according to the procedure of the kit (Solarbio).

Animals. Male C57BL/6 mice (22–25 g) were purchased from the Charles River Co., Ltd. All animal experiments were performed in accordance with the Guide for the Care and Use of Laboratory Animals. All the related protocols were approved by the Animal Ethics Committee of Xiamen University (Xiamen, China). Mice were housed in sterile cages (5 mice/cage) and ventilated in a pathogen-free room with a laminar flow hood, a 12 h light/12 h dark cycle, and fed with standard chow and water. All animals were kept sterile throughout the experiment.

Establishment of transient Middle Cerebral Artery Occlusion (tMCAO) stroke models. After the mice were anaesthetized, the skin of their necks was cut with scissors to expose the common carotid artery (CCA). The sheath of the artery was carefully separated so as not to injure the vagus nerve. The external carotid artery (ECA) and internal carotid artery (ICA) were separated. The CCA and ECA were ligated with silk thread. An uncoated nylon monofilament (Beijing Cinontech Co. Ltd. China) was inserted through CCA into the ICA and removed after 30 min of occlusion. Achievement of ischemia was confirmed by monitoring regional cerebral blood flow using laser speckle contrast imaging. Animals without at least 80 % reduction in cerebral blood flow were excluded from the study. Sham-operated animals underwent the same experimental conditions except that the filament structure was not implanted. The successful establishment of the mouse tMCAO model was confirmed by TTC staining. Coronal sections (2 mm thick) of brain tissue were prepared and stained with 2 % TTC. Brain sections were fixed in 10 % formalin. The areas without red staining were considered as infarct area.

***In vivo* FL imaging.** The Anti-TRAIL-ICG or free ICG (1 mg/kg) was *i.v.* injected into mice (n = 3, in each group) through the tail-vein, then FL images were acquired at different time points by an *in vivo* FL imaging system (Caliper IVIS Lumina II, USA). In addition, typical organs were collected at 4 h after administration of Anti-TRAIL-ICG nanoagent to examine the biodistribution profile in tMCAO mice.

***In vivo* PA imaging.** Mice were anaesthetized with 2.5 % isoflurane and secured on a heated imaging platform under the PA imaging transducer. US gel was applied to the top of the brain to facilitate US transmission. Experimental PA imaging with co-registered US was performed using a commercially available laser-integrated high-frequency US system (Vevo® LAZR, FujiFilm VisualSonics Inc.). The ultrasonic probe type is MX250, center frequency 18–26 MHz. The system consists of a tunable NIR Nd:YAG laser coupled into two fiber bundles, which are tightly attached to a 256 element linear array ultrasound transducer on either side. The laser signal synchronised the acquisition of the US signal. The excitation wavelength was 780 nm. Animals were removed and monitored to ensure full recovery at the end of imaging.

Neurological deficit score (NDS). Longa scores were used to assess the motor function. 0 points: no signs of nerve damage; 1 point: inability to fully extend the fore or hind paw on the opposite side of the operation; 2 points: turning to the opposite side of the operation when walking; 3 points: falling to the opposite side of the operation when walking; 4 points: unable to walk spontaneously, loss of consciousness.

***In vivo* MRI.** The MRI was performed at 24 h after tMCAO with a 9.4 T MR scanner (Biospec, Bruker) by using multi-slice and multi-echo sequence with the following parameters: slices: 20; slice thickness: 0.5 mm; field of view: 2 × 2 cm^2; matrix size: 256 × 256. Infarct volume was calculated from all T2-weighted images. The infarct rate was calculated to avoid the effect of oedema, the infarct rate = infarct volume/contralateral hemisphere volume × 100 %.

***In vivo* OCTA imaging.** To better understand the therapeutic effects of nanoagent on the cerebral microvasculature after stroke, a home-built swept-source OCT angiography system was used to study changes in microvascular morphology before tMCAO and after treatment in different groups. The light source of the system was a high-speed swept laser with a center wavelength of l064 nm, and repetition rate of 200 kHz with the full width at half maximum of 100 nm. This system has an axial resolution of approximately 5 μm and a lateral resolution of approximately 29 μm. The system's imaging FOV is adjustable according to the actual imaging area, and the imaging depth in the air is approximately 2–3 mm. Briefly, this system can provide a wide field of view (FOV) of approximately 10 mm × 10 mm with 400 A-lines in each B-scan (fast axis X direction). The C-scan (slow axis Y direction) contained 2400 B-scans with four repeated scans at the same B-scan area. Mice were anaesthetized with 2.5 % isoflurane. During the OCTA imaging, the mouse was fixed on a high-precision head immobilizer to acquire the optimal imaging position and reduce the motion artifacts. A heating pad was utilized to maintain the body temperature of the mouse during imaging.

Measurement of MDA expression. On the third day after stroke, the brains of the mice were removed after cardiac perfusion. Isolated right brain tissue was homogenized by adding the extraction solution. The supernatant was then collected after centrifugation at 8500 rpm for 10 min and the absorbance was measured at 532 and 600 nm using a microplate reader. The MDA level was calculated according to the formula in the specification (Solarbio).

Nissl staining. Isolated brain tissue after cardiac perfusion was embedded in paraffin and sectioned at 4 μm. Paraffin sections were then stained with toluidine blue (Servicebio).

Immunohistochemistry. Paraffin sections were incubated with GPX4 antibody (1:3000, Servicebio) at 4 °C overnight, then incubated with secondary antibody at room temperature for 30 min in the dark after washing with PBST and visualized with DAB solution. Finally, the nucleus was counterstained with hematoxylin and the sections were digitally scanned.

Hematoxylin and eosin staining. Organs were fixed in 4 % paraformaldehyde solution after cardiac perfusion, embedded in paraffin and sectioned at 8 μm. H&E staining was performed according to specifications (Servicebio) and observed under the microscope.

Statistical analysis. Data are presented as the mean ± standard deviation (SD). Statistical analysis of the data was performed by one-way analysis of variance (ANOVA). In addition, a $p < 0.05$ was considered to be statistically significant.

CRediT authorship contribution statement

Qiong Yang: Writing – review & editing, Writing – original draft, Visualization, Formal analysis, Data curation, Conceptualization. **Wenxuan Ye:** Writing – review & editing, Supervision, Project administration. **Doudou Luo:** Investigation, Conceptualization. **Jiwei Xing:** Validation, Investigation. **Qingqing Xiao:** Resources, Funding acquisition. **Huiling Wu:** Project administration. **Youliang Yao:** Supervision. **Guangxing Wang:** Writing – original draft, Supervision. **Luyao Yang:** Writing – original draft. **Dongbei Guo:** Supervision. **Kun Wang:** Supervision. **Yaqin He:** Supervision, Funding acquisition. **Xiaofeng Ye:** Investigation, Funding acquisition. **Jinde Zhang:** Investigation, Funding acquisition. **Zhaokui Jin:** Visualization, Supervision, Investigation. **Zhongxiong Fan:** Writing – original draft, Visualization. **Xiaofei Wen:** Supervision, Funding acquisition, Data curation. **Jingsong Mao:** Visualization, Supervision, Funding acquisition, Conceptualization. **Xiaoyuan Chen:** Supervision. **Qingliang Zhao:** Writing – review & editing, Supervision, Conceptualization.

Declaration of competing interest

The authors declare that they have no known competing financial interests or personal relationships that could have appeared to influence the work reported in this paper.

Data availability

Data will be made available on request.

Acknowledgements

This work was supported by grants from the State Key Laboratory of Vaccines for Infectious Diseases, Xiang An Biomedicine Laboratory (2023XAKJ0101031), Fundamental Research Funds for the Central Universities of China (20720210117), Fujian Province Science and Technology Plan Guiding Project (2022Y0002), National Natural Science Foundation of China (81971665, 82360360), Natural Science Foundation of Fujian Province (2021J011366, 2020J01158, 2022J01019), Medical and Health Guidance Project of Xiamen (3502Z20214ZD1016), and Xiamen Health High-Level Talent Training Program. Ningxia Hui Autonomous Region Key Research and Development Program (2022BEG03127), the Key research and development program in Xinjiang Uygur Autonomous Region (2023B02030 and 2023B02030-1), National Natural Science Foundation of China (62005048), Natural Science Foundation of Guangxi (2023GXNSFAA026023), Central Government Guided Local Science and Technology Development Fund Projects (2023ZYZX 1090), Ministry of Education Industry-university Cooperative Education Project (220606053295218).

Appendix A. Supplementary data

Supplementary data to this article can be found online at https://doi.org/10.1016/j.mtbio.2024.101094.

References

[1] V.L. Feigin, B.A. Stark, C.O. Johnson, G.A. Roth, C. Bisignano, G.G. Abady, et al., Global, regional, and national burden of stroke and its risk factors, 1990–2019: a systematic analysis for the Global Burden of Disease Study 2019, Lancet Neurol. 20 (10) (2021) 795–820.
[2] C.W. Tsao, A.W. Aday, Z.I. Almarzooq, A. Alonso, A.Z. Beaton, M.S. Bittencourt, et al., Heart disease and stroke Statistics—2022 update: a report from the American heart association, Circulation 145 (8) (2022).
[3] Y. Zhao, X. Zhang, X. Chen, Y. Wei, Neuronal injuries in cerebral infarction and ischemic stroke: from mechanisms to treatment, Int. J. Mol. Med. 49 (2) (2021) (Review).
[4] S. Prabhakaran, I. Ruff, R.A. Bernstein, Acute stroke intervention, JAMA 313 (14) (2015).
[5] Y.H. Zhao, B. Yuan, J. Chen, D.H. Feng, B. Zhao, C. Qin, et al., Endothelial progenitor cells: therapeutic perspective for ischemic stroke, CNS Neurosci. Ther. 19 (2) (2012) 67–75.
[6] B.C.V. Campbell, D.A. De Silva, M.R. Macleod, S.B. Coutts, L.H. Schwamm, S. M. Davis, et al., Ischaemic stroke, Nat. Rev. Dis. Prim. 5 (1) (2019).
[7] W. Hacke, M. Kaste, E. Bluhmki, M. Brozman, A. Dávalos, D. Guidetti, et al., Thrombolysis with alteplase 3 to 4.5 hours after acute ischemic stroke, N. Engl. J. Med. 359 (13) (2008) 1317–1329.
[8] M. Haupt, S.T. Gerner, M. Bähr, T.R. Doeppner, Neuroprotective strategies for ischemic stroke—future perspectives, Int. J. Mol. Sci. 24 (5) (2023).
[9] R.G. Nogueira, H.L. Lutsep, R. Gupta, T.G. Jovin, G.W. Albers, G.A. Walker, et al., Trevo versus Merci retrievers for thrombectomy revascularisation of large vessel occlusions in acute ischaemic stroke (TREVO 2): a randomised trial, Lancet 380 (9849) (2012) 1231–1240.
[10] J.L. Saver, R. Jahan, E.I. Levy, T.G. Jovin, B. Baxter, R.G. Nogueira, et al., Solitaire flow restoration device versus the Merci Retriever in patients with acute ischaemic stroke (SWIFT): a randomised, parallel-group, non-inferiority trial, Lancet 380 (9849) (2012) 1241–1249.
[11] W.S. Smith, G. Sung, J. Saver, R. Budzik, G. Duckwiler, D.S. Liebeskind, et al., Mechanical thrombectomy for acute ischemic stroke, Stroke 39 (4) (2008) 1205–1212.
[12] W.S. Smith, G. Sung, S. Starkman, J.L. Saver, C.S. Kidwell, Y.P. Gobin, et al., Safety and efficacy of mechanical embolectomy in acute ischemic stroke, Stroke 36 (7) (2005) 1432–1438.
[13] X. Xiao, Y. Gao, S. Liu, M. Wang, M. Zhong, J. Wang, et al., A "nano-courier" for precise delivery of acetylcholine and melatonin by C5a-targeted aptamers effectively attenuates reperfusion injury of ischemic stroke, Adv. Funct. Mater. 33 (23) (2023).
[14] A. Moretti, F. Ferrari, R.F. Villa, Neuroprotection for ischaemic stroke: current status and challenges, Pharmacol. Therapeut. 146 (2015) 23–34.
[15] L. Ugalde-Triviño, M. Díaz-Guerra, PSD-95: an effective target for stroke therapy using neuroprotective peptides, Int. J. Mol. Sci. 22 (22) (2021).
[16] B.J. Gwag, Y.A. Lee, S.Y. Ko, M.J. Lee, D.S. Im, B.S. Yun, et al., Marked prevention of ischemic brain injury by Neu2000, an NMDA antagonist and antioxidant derived from aspirin and sulfasalazine, J. Cerebr. Blood Flow Metabol. 27 (6) (2006) 1142–1151.
[17] A. Aliena-Valero, J. Baixauli-Martín, M. Castelló-Ruiz, G. Torregrosa, D. Hervás, J. B. Salom, Effect of uric acid in animal models of ischemic stroke: a systematic review and meta-analysis, J. Cerebr. Blood Flow Metabol. 41 (4) (2020) 707–722.
[18] H. Jiao, Z. Wang, Y. Liu, P. Wang, Y. Xue, Specific role of tight junction proteins claudin-5, occludin, and ZO-1 of the blood–brain barrier in a focal cerebral ischemic insult, J. Mol. Neurosci. 44 (2) (2011) 130–139.
[19] Y. Yang, E.Y. Estrada, J.F. Thompson, W. Liu, G.A. Rosenberg, Matrix metalloproteinase-mediated disruption of tight junction proteins in cerebral vessels is reversed by synthetic matrix metalloproteinase inhibitor in focal ischemia in rat, J. Cerebr. Blood Flow Metabol. 27 (4) (2006) 697–709.
[20] T. Kulik, Y. Kusano, S. Aronhime, A.L. Sandler, H.R. Winn, Regulation of cerebral vasculature in normal and ischemic brain, Neuropharmacology 55 (3) (2008) 281–288.
[21] R. Cecchelli, V. Berezowski, S. Lundquist, M. Culot, M. Renftel, M.-P. Dehouck, et al., Modelling of the blood–brain barrier in drug discovery and development, Nat. Rev. Drug Discov. 6 (8) (2007) 650–661.
[22] J. Yuan, L. Li, Q. Yang, H. Ran, J. Wang, K. Hu, et al., Targeted treatment of ischemic stroke by bioactive nanoparticle-derived reactive oxygen species responsive and inflammation-resolving nanotherapies, ACS Nano 15 (10) (2021) 16076–16094.
[23] J.J.E. Mulvihill, E.M. Cunnane, A.M. Ross, J.T. Duskey, G. Tosi, A.M. Grabrucker, Drug delivery across the blood–brain barrier: recent advances in the use of nanocarriers, Nanomedicine 15 (2) (2020) 205–214.
[24] E. Neuwelt, N.J. Abbott, L. Abrey, W.A. Banks, B. Blakley, T. Davis, et al., Strategies to advance translational research into brain barriers, Lancet Neurol. 7 (1) (2008) 84–96.
[25] S.H.M. Wong, W.Y. Kong, C.-M. Fang, H.-S. Loh, L.-H. Chuah, S. Abdullah, et al., The TRAIL to cancer therapy: hindrances and potential solutions, Crit. Rev. Oncol. Hematol. 143 (2019) 81–94.
[26] H. Dianat-Moghadam, M. Heidarifard, A. Mahari, M. Shahgolzari, M. Keshavarz, M. Nouri, et al., TRAIL in oncology: from recombinant TRAIL to nano- and self-targeted TRAIL-based therapies, Pharmacol. Res. 155 (2020).
[27] X. Yuan, A. Gajan, Q. Chu, H. Xiong, K. Wu, G.S. Wu, Developing TRAIL/TRAIL death receptor-based cancer therapies, Cancer Metastasis Rev. 37 (4) (2018) 733–748.
[28] G. Cantarella, G. Pignataro, G. Di Benedetto, S. Anzilotti, A. Vinciguerra, O. Cuomo, et al., Ischemic tolerance modulates TRAIL expression and its receptors and generates a neuroprotected phenotype, Cell Death Dis. 5 (7) (2014) e1331-e1331.
[29] A. Weiland, Y. Wang, W. Wu, X. Lan, X. Han, Q. Li, et al., Ferroptosis and its role in diverse brain diseases, Mol. Neurobiol. 56 (7) (2018) 4880–4893.
[30] Q.z. Tuo, P. Lei, K.A. Jackman, X.l. Li, H. Xiong, X.l. Li, et al., Tau-mediated iron export prevents ferroptotic damage after ischemic stroke, Mol. Psychiatr. 22 (11) (2017) 1520–1530.
[31] A. Datta, D. Sarmah, L. Mounica, H. Kaur, R. Kesharwani, G. Verma, et al., Cell death pathways in ischemic stroke and targeted pharmacotherapy, Translational Stroke Research 11 (6) (2020) 1185–1202.
[32] J.H. Kim, A.J. Najy, J. Li, X. Luo, H.R.C. Kim, M.H.A. Choudry, et al., Involvement of Bid in the crosstalk between ferroptotic agent-induced ER stress and TRAIL-induced apoptosis, J. Cell. Physiol. 237 (11) (2022) 4180–4196.
[33] K.-J. Park, C.-H. Lee, A. Kim, K.J. Jeong, C.-H. Kim, Y.-S. Kim, Death receptors 4 and 5 activate Nox1 NADPH oxidase through riboflavin kinase to induce reactive oxygen species-mediated apoptotic cell death, J. Biol. Chem. 287 (5) (2012) 3313–3325.
[34] S. Kaviarasi, E. Yuba, A. Harada, U.M. Krishnan, Emerging paradigms in nanotechnology for imaging and treatment of cerebral ischemia, J. Contr. Release 300 (2019) 22–45.
[35] S. Nozohouri, A.E. Sifat, B. Vaidya, T.J. Abbruscato, Novel approaches for the delivery of therapeutics in ischemic stroke, Drug Discov. Today 25 (3) (2020) 535–551.
[36] V.N. Bharadwaj, D.T. Nguyen, V.D. Kodibagkar, S.E. Stabenfeldt, Nanoparticle-based therapeutics for brain injury, Adv. Healthcare Mater. 7 (1) (2017).
[37] Y. Wen, W. Zhang, N. Gong, Y.-F. Wang, H.-B. Guo, W. Guo, et al., Carrier-free, self-assembled pure drug nanorods composed of 10-hydroxycamptothecin and chlorin e6 for combinatorial chemo-photodynamic antitumor therapy in vivo, Nanoscale 9 (38) (2017) 14347–14356.
[38] L. Zhang, X. Zhang, G. Lu, F. Li, W. Bao, C. Song, et al., Cell membrane camouflaged hydrophobic drug nanoflake sandwiched with photosensitizer for orchestration of chemo-photothermal combination therapy, Small 15 (20) (2019).
[39] K. Xue, H. Tian, F. Zhu, F. Wang, Z. Fan, Q. Zhao, et al., Ultralong-circulating and self-targeting "watson–crick A = t"-inspired supramolecular nanotheranostics for NIR-II imaging-guided photochemotherapy, ACS Appl. Mater. Interfaces 12 (29) (2020) 32477–32492.

[40] M.B. Reinhart, C.R. Huntington, L.J. Blair, B.T. Heniford, V.A. Augenstein, Indocyanine green, Surg. Innovat. 23 (2) (2015) 166–175.
[41] E. Cassinotti, L. Boni, L. Baldari, Application of indocyanine green (ICG)-guided surgery in clinical practice: lesson to learn from other organs—an overview on clinical applications and future perspectives, Updates in Surgery 75 (2) (2022) 357–365.
[42] M. Zhu, Z. Sheng, Y. Jia, D. Hu, X. Liu, X. Xia, et al., Indocyanine green-holo-transferrin nanoassemblies for tumor-targeted dual-modal imaging and photothermal therapy of glioma, ACS Appl. Mater. Interfaces 9 (45) (2017) 39249–39258.
[43] K.E. Wilson, S.V. Bachawal, L. Abou-Elkacem, K. Jensen, S. Machtaler, L. Tian, et al., Spectroscopic photoacoustic molecular imaging of breast cancer using a B7-H3-targeted ICG contrast agent, Theranostics 7 (6) (2017) 1463–1476.
[44] J. Lv, S. Li, J. Zhang, F. Duan, Z. Wu, R. Chen, et al., In vivo photoacoustic imaging dynamically monitors the structural and functional changes of ischemic stroke at a very early stage, Theranostics 10 (2) (2020) 816–828.
[45] K.K. Haga, L.J. Gregory, C.A. Hicks, M.A. Ward, J.S. Beech, P.W. Bath, et al., The neuronal nitric oxide synthase inhibitor, TRIM, as a neuroprotective agent: effects in models of cerebral ischaemia using histological and magnetic resonance imaging techniques, Brain Res. 993 (1–2) (2003) 42–53.
[46] X.R. Shao, X.Q. Wei, X. Song, L.Y. Hao, X.X. Cai, Z.R. Zhang, et al., Independent effect of polymeric nanoparticle zeta potential/surface charge, on their cytotoxicity and affinity to cells, Cell Prolif. 48 (4) (2015) 465–474.
[47] C.I. Tasca, T. Dal-Cim, H. Cimarosti, In vitro oxygen-glucose deprivation to study ischemic cell death, in: Neuronal Cell Death, 2015, pp. 197–210.
[48] A. Almasan, A. Ashkenazi, Apo2L/TRAIL: apoptosis signaling, biology, and potential for cancer therapy, Cytokine Growth Factor Rev. 14 (3–4) (2003) 337–348.
[49] P.P.G. Guimarães, S. Gaglione, T. Sewastianik, R.D. Carrasco, R. Langer, M. J. Mitchell, Nanoparticles for immune cytokine TRAIL-based cancer therapy, ACS Nano 12 (2) (2018) 912–931.
[50] G. Cantarella, N. Risuglia, G. Lombardo, L. Lempereur, F. Nicoletti, M. Memo, et al., Protective effects of estradiol on TRAIL-induced apoptosis in a human oligodendrocytic cell line: evidence for multiple sites of interactions, Cell Death Differ. 11 (5) (2004) 503–511.
[51] G. Cantarella, D. Uberti, T. Carsana, G. Lombardo, R. Bernardini, M. Memo, Neutralization of TRAIL death pathway protects human neuronal cell line from β-amyloid toxicity, Cell Death Differ. 10 (1) (2003) 134–141.
[52] H. Lin, Y. Zhou, J. Wang, H. Wang, T. Yao, H. Chen, et al., Repurposing ICG enables MR/PA imaging signal amplification and iron depletion for iron-overload disorders, Sci. Adv. 7 (51) (2021).
[53] H. Lin, S. Li, J. Wang, C. Chu, Y. Zhang, X. Pang, et al., A single-step multi-level supramolecular system for cancer sonotheranostics, Nanoscale Horizons 4 (1) (2019) 190–195.
[54] R. Yue, C. Zhang, L. Xu, Y. Wang, G. Guan, L. Lei, et al., Dual key co-activated nanoplatform for switchable MRI monitoring accurate ferroptosis-based synergistic therapy, Chem 8 (7) (2022) 1956–1981.
[55] Y. Yuan, Y. Zheng, X. Zhang, Y. Chen, X. Wu, J. Wu, et al., BNIP3L/NIX-mediated mitophagy protects against ischemic brain injury independent of PARK2, Autophagy 13 (10) (2017) 1754–1766.
[56] G.C. Terstappen, A.H. Meyer, R.D. Bell, W. Zhang, Strategies for delivering therapeutics across the blood–brain barrier, Nat. Rev. Drug Discov. 20 (5) (2021) 362–383.
[57] D. Huang, G. Wang, J. Mao, C. Liu, Z. Fan, Y. Zhang, et al., Intravital whole-process monitoring thermo-chemotherapy via 2D silicon nanoplatform: a macro guidance and long-term microscopic precise imaging strategy, Adv. Sci. 8 (16) (2021).
[58] J.-S. Kang, M.-H. Lee, Overview of therapeutic drug monitoring, The Korean journal of internal medicine 24 (1) (2009).
[59] H.C. Ates, J.A. Roberts, J. Lipman, A.E.G. Cass, G.A. Urban, C. Dincer, On-site therapeutic drug monitoring, Trends Biotechnol. 38 (11) (2020) 1262–1277.
[60] X. Ma, B. Zhang, N. Ma, C. Liu, Y. Miao, X. Liang, et al., Unveiling the mechanism of alleviating ischemia reperfusion injury via a layered double hydroxide-based nanozyme, ACS Appl. Mater. Interfaces (2023).
[61] P. Carmeliet, Blood vessels and nerves: common signals, pathways and diseases, Nat. Rev. Genet. 4 (9) (2003) 710–720.
[62] A. Taguchi, T. Soma, H. Tanaka, T. Kanda, H. Nishimura, H. Yoshikawa, et al., Administration of CD34+ cells after stroke enhances neurogenesis via angiogenesisin a mouse model, J. Clin. Invest. 114 (3) (2004) 330–338.
[63] L. Beckmann, X. Zhang, N.A. Nadkarni, Z. Cai, A. Batra, D.P. Sullivan, et al., Longitudinal deep-brain imaging in mouse using visible-light optical coherence tomography through chronic microprism cranial window, Biomed. Opt Express 10 (10) (2019).
[64] W.J. Choi, Y. Li, R.K. Wang, Monitoring acute stroke progression: multi-parametric OCT imaging of cortical perfusion, flow, and tissue scattering in a mouse model of permanent focal ischemia, IEEE Trans. Med. Imag. 38 (6) (2019) 1427–1437.
[65] F. Hong, X. Geng, G. Min, X. Sun, B. Zhang, Y. Yao, et al., Deep NIR-II optical imaging combined with minimally invasive interventional photothermal therapy for orthotopic bladder cancer, Chem. Eng. J. 449 (2022).
[66] J. Lee, Y. Gursoy-Ozdemir, B. Fu, D.A. Boas, T. Dalkara, Optical coherence tomography imaging of capillary reperfusion after ischemic stroke, Appl. Opt. 55 (33) (2016).
[67] Y. Zhang, J. Li, C. Liu, K. Zheng, B. Zhang, Y. Zhou, et al., Development of a multi-scene universal multiple wavelet-FFT algorithm (MW-FFTA) for denoising motion artifacts in OCT-angiography in vivo imaging, Opt Express 30 (20) (2022).